松科二井早白垩世早期玄武安山岩的发现及地质意义*

张钊 黄丰** 许继峰 曾云川 张丽莹 杨旭立 张蔓

ZHANG Zhao, HUANG Feng**, XU JiFeng, ZENG YunChuan, ZHANG LiYing, YANG XuLi and ZHANG Man

中国地质大学地质过程与矿产资源国家重点实验室, 地球科学与资源学院, 北京 100083

State Key Laboratory of Geological Processes and Mineral Resources, and School of Earth Science and Resources, China University of Geosciences, Beijing 100083, *China*

2021-12-30 收稿, 2022-04-20 改回.

Zhang Z, Huang F, Xu JF, Zeng YC, Zhang LY, Yang XL and Zhang M. 2022. Discovery and geological implications of the Early Cretaceous basaltic andesites in SK2 borehole. *Acta Petrologica Sinica*, 38(6):1756 – 1770, doi:10.18654/1000-0569/2022.06.14

Abstract A continuous sedimentary-volcanic core of Songliao Basin has been obtained through ultra-deep drilling of the SK2 borehole, which provides excellent materials for systematically investigating the formation of the Songliao Basin and the tectonic evolution history of Northeast China. In this study, we conducted a combined study of zircon U-Pb dating, whole-rock geochemical and Sr-Nd isotopic analysis on basaltic andesite samples from SK2 borehole with depths ranging from –6035m to –6084m. These SK2 basaltic andesite samples belong to Huoshiling Formation and they were formed at Early Cretaceous (141.6 ± 1.4Ma) according to the zircon U-Pb dating results. The SK2 basaltic andesites are enriched in large ion lithophile elements, depleted in high field strength elements, and their geochemical signatures are consistent with arc magmas. These rocks show depleted Sr-Nd isotope characteristics ($(^{87}Sr/^{86}Sr)_i$ = 0.70496 ~ 0.70478, $\varepsilon_{Nd}(t)$ = 1.05 ~ 1.61), suggesting a depleted mantle source. In the Early Cretaceous, the evolution of Northeast China was mainly controlled by the southward subduction of the Mongol-Okhotsk oceanic plate and the western subduction of the Paleo-Pacific Plate. Previous study has shown that the subduction of Mongolia-Okhotsk Ocean induced coeval magmatism in the Great Xing'an Range, however, it is not clear whether its influence extends into the Songliao Basin. The initial subduction of Paleo-Pacific lithosphere may induce Late Mesozoic magmatism in the west of Songliao Basin. The Early Cretaceous formation and evolution of Songliao Basin were mainly affected by the activities of Mongolia Okhotsk Ocean or Paleo-Pacific lithosphere remains controversial. The Th/Hf (1.10 ~ 2.87) and Zr/Y ratios (10.1 ~ 18.7) of the SK2 basaltic andesites are similar to the within-plate basaltic magmas, we therefore suggest that SK2 samples belong to intraplate magmatism. The samples also show higher Zr, Hf and Ti contents, higher Nb/Ta ratios and more depleted Nd isotope compositions than the coeval mafic rocks in the Great Xing'an Range, indicating the SK2 samples formed in a different tectonic background. Accordingly, the Early Cretaceous volcanic rocks in Songliao Basin are most likely occurred by rollback of the subducting Paleo-Pacific Plate, while incidental lithospheric extension may promote the formation of Songliao Basin.

Key words Songliao Basin; SK2 borehole; Early Cretaceous; Basaltic andesite; Rollback of the Paleo-Pacific Plate

摘 要 松科二井超深钻探获取了松辽盆地连续沉积-火山岩心,为系统研究中生代松辽盆地形成机制、揭示中国东北地区构造演化历史提供了极好的研究材料。本文对取自松科二井井深 –6035 ~ –6084m 的玄武安山岩开展了系统的锆石 U-Pb 定年、全岩主微量元素和 Sr-Nd 同位素分析测试。研究结果表明,松科二井玄武安山岩隶属于火石岭组底部,其形成时代为早白垩世早期(141.6 ± 1.4Ma)。玄武安山岩样品富集大离子亲石元素,亏损高场强元素,具有弧岩浆的地球化学特征。这些样品

* 本文受国家重点研发计划项目(2020YFA0714800、2019YFC0605405)、国家自然科学基金项目(41790453、41973027)和中央高校基本科研业务费(2652019054)联合资助.

第一作者简介:张钊,男,1995 生,博士生,矿物学,岩石学,矿床学专业,E-mail:unitize@126.com

** **通讯作者**:黄丰,男,1988 年生,博士,副教授,地球化学专业,E-mail:fenghuang@cugb.edu.cn

显示了一定程度的轻重稀土元素分异($(La/Yb)_N = 8.40 \sim 11.88$),具有轻微亏损的 Sr-Nd 同位素特征($(^{87}Sr/^{86}Sr)_i = 0.70496 \sim 0.70478$,$\varepsilon_{Nd}(t) = 1.05 \sim 1.61$),表明它们很可能源自于岩石圈地幔。早白垩世时期中国东北地区主要受控于蒙古-鄂霍茨克洋的南向俯冲和东侧古太平洋俯冲过程,目前研究揭示了前者影响了同期的大兴安岭地区的火山活动,但其影响范围是否延伸至松辽盆地内部尚不清楚。古太平洋岩石圈开始俯冲后很可能诱发了松辽盆地西侧晚中生代火山岩的形成。早白垩世松辽盆地演化主要受蒙古-鄂霍茨克洋还是古太平洋板块的活动影响仍存在较多争议。松科二井玄武安山岩具有与板内玄武岩相近的 Th/Hf 比值(1.10 ~ 2.87)及 Zr/Y 比值(10.1 ~ 18.7),表明它们具有板内岩浆的地球化学特征,且松科二井样品比同时代盆地西部的大兴安岭地区玄武岩具有更高的 Nb/Ta 比值,更高的 Zr、Hf 与 Ti 含量,以及更亏损的 Nd 同位素特征,可能指示与大兴安岭地区玄武岩形成于不同的构造背景。松辽盆地内早白垩世火山岩很可能为古太平洋板片回转诱发形成,指示早白垩世古太平洋板片回转诱发的岩石圈伸展促进了松辽盆地的形成。

关键词 松辽盆地;松科二井;早白垩世早期;玄武安山岩;古太平洋板片回转

中图法分类号 P588.144; P597.3

沉积盆地的成岩成矿研究一直是国内外关注的热点之一(Chen and Chang, 1994; Wang *et al.*, 2016)。松辽盆地是中国东北地区存在时间最长,最大的白垩纪含油气陆相沉积盆地,其面积达 260000km^2,横跨黑龙江、吉林和辽宁三省(Wang *et al.*, 2013)。它保存了中生代良好的火山-沉积记录,是研究中生代全球气候环境变化,白垩纪温室效应,寻找深部能源资源,探讨大庆油田成因并丰富陆相生油理论,揭示中国东北构造演化历史以及松辽盆地的形成机制的重要天然实验室(Chen and Chang, 1994; Wang *et al.*, 2013)。松科二井获取了松辽盆地深至地下 7018m,总长 4134.81m 的连续岩心,是亚洲最深的科学钻井(侯贺晟等,2018)。其钻遇地层包含上白垩统明水村组、四方台组、嫩江组、姚家组、青山口组,及下白垩统至上侏罗统的登娄库组、营城组、沙河子组及火石岭组。前人对松辽盆地早白垩世钻井样品的研究表明,盆地内火山活动集中于火石岭组与营城组中(Wang *et al.*, 2006a, 2002; Li *et al.*, 2019)。营城组流纹岩与安山岩分布范围广泛,在盆地南部的长岭断陷与盆地北部徐家围子断陷,盆地西缘,以及松科二井中均有报导(许文良等,2013; Chang *et al.*, 2017),其时代为 115 ~ 102Ma (Chang *et al.*, 2017)。营城组出露的 A 型流纹岩源自深部地壳的部分熔融,其中的出露的埃达克质岩暗示地幔上涌及岩石圈拆沉可能影响了该时期松辽盆地演化(Wu *et al.*, 2002; Xu *et al.*, 2002;许文良等,2013; Ji *et al.*, 2019a)。但是对于侏罗-白垩纪之交松辽盆地的形成和演化历史尚不清楚,该时期盆地底部主要为火石岭组沉积岩夹少量中基性火山岩。前人对其火石岭组形成时代存在两种认识:133 ~ 125Ma (裴福萍等,2008;袁伟等,2014;Chang *et al.*, 2017; Wang *et al.*, 2017)与 150 ~ 140Ma (Wang *et al.*, 2002; 瞿雪姣等 2014)。截至目前,对火石岭组火山岩没有很好的年代学和岩石成因限制,这严重制约了人们对松辽盆地早期形成过程的认识。本文通过对取自松科二井深 -6035m ~ -6084m 火石岭组中的玄武安山岩进行年代学和地球化学研究,初步确定其时代及岩石成因,反映了古太平洋俯冲对中国东北的影响,尝试揭示松辽盆地形成早期演化过程。

1 地质背景与样品描述

中国东北地区位于中亚造山带东段,向南以索伦-西拉木伦-长春-延吉断裂与华北板块分隔,向西北以蒙古-鄂霍茨克缝合带与西伯利亚克拉通分隔(图 1; Wu *et al.*, 2011; Xu *et al.*, 2013; Liu *et al.*, 2017)。以深大断裂为界,中国东北由多个微陆块组成,自西北向东南依次为额尔古纳地块、兴安地块、松嫩地块、佳木斯地块和兴凯地块(Xiao *et al.*, 2003, 2009; Li, 2006),大部分地块被认为是从冈瓦纳大陆北缘(Wilde and Zhou, 2015)或西伯利亚克拉通(Zhou *et al.*, 2015)分离出来的。中国东北各微陆块碰撞拼合集中于古生代时期,其中额尔古纳地块与兴安地块于 510 ~ 490Ma 拼合于新林-喜桂图缝合带(葛文春等, 2007;Miao *et al.*, 2015),兴安地块与松嫩-张广才岭地块于早石炭世拼合(Li *et al.*, 2014; Liu *et al.*, 2017),松嫩与佳木斯地块拼合始于早古生代,结束于中侏罗世(Wang *et al.*, 2012; Liu *et al.*, 2017)。早-中三叠世,古亚洲洋呈“剪刀式”闭合后中国东北与华北地块碰撞(Wang *et al.*, 2018; Li *et al.*, 2020)。中国东北中生代构造演化转变为受东部环太平洋构造域及西北部蒙古-鄂霍茨克洋俯冲闭合的叠加影响,发育了众多伸展断陷盆地和大量火山岩(Xu *et al.*, 2009; Huang *et al.*, 2017; Li *et al.*, 2021; Wang *et al.*, 2022; Zhu *et al.*, 2022)。

松辽盆地位于中国东北中部的松嫩地块之上,长 750km、宽 330 ~ 370km,为白垩纪最大陆相含油气沉积盆地(Wang *et al.*, 2016; Li *et al.*, 2020)。其基底主要由浅变质的古生代和中生代花岗岩类以及前寒武纪地层构成(Wang *et al.*, 2014)。根据盆地内三个角度不整合面,可将盆地划分为:(1)同裂谷期(150 ~ 110Ma),包括火石岭组中基性火山岩、沙河子组沙泥岩和营城组中酸性火山岩;(2)后裂谷期(110 ~ 79.1Ma),包括登娄库组、泉头组、青山口组、姚家及嫩江组的巨厚层沉积岩;(3)构造反转期(79.1 ~ 64Ma),包括四方台组与明水村组(Wang *et al.*, 2016; Li *et al.*, 2021)。

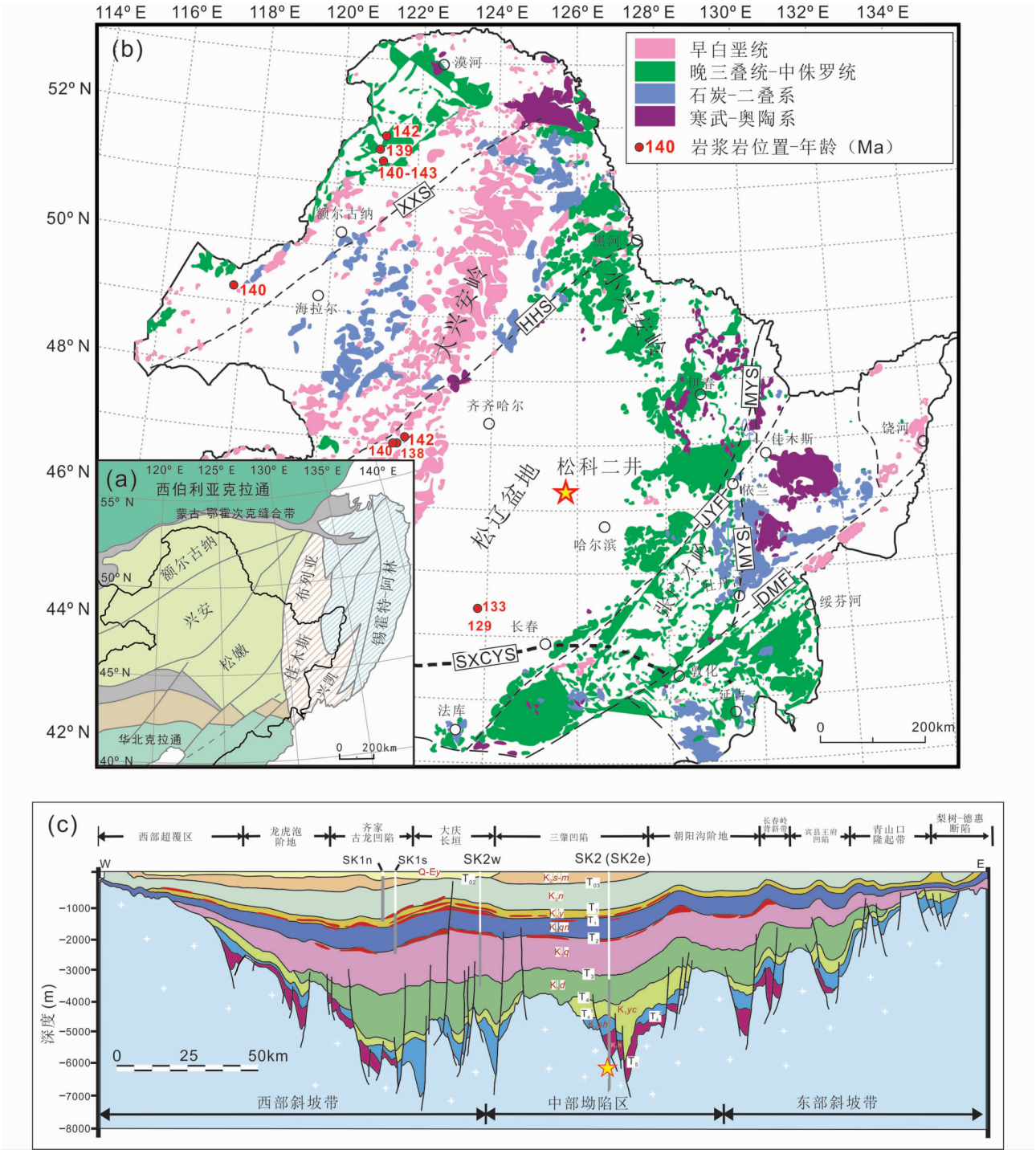

图 1　中国东北地区构造单元、地质简图和松辽盆地纵剖面图

(a)中国东北主要构造单元示意图；(b)古生代-中生代岩浆分布(据 Wu *et al.*, 2011 与 Xu *et al.*, 2013 修改)；(c)基于地震分析松辽盆地构造剖面. SK1n、SK1s、SK2w 和 SK2(或 SK2e)中的灰色带为取芯层段,白色带为未取芯层段(据 Wang *et al.*, 2013 修改). 早白垩世早期中基性岩引自 Wang *et al.* (2006b), Zhang *et al.* (2008), Yang *et al.* (2015a), Ying *et al.* (2010), 崔玉斌等(2021), 吴涛涛等(2018)和裴福萍等(2008). 缩写:XXS-新林-喜桂图缝合带;HHS-黑河-贺根山缝合带;MYS-牡丹江-依兰缝合带;SXCYS-索伦-西拉木伦-长春-延吉缝合带;JYF-佳木斯-延吉断裂;DMF-敦化-密山断裂;NT-那达哈达增生地体;Q-Ey-第四纪/新近纪;K_2s-四方台组;K_2m-明水组;K_2n-嫩江组;K_2y-姚家组;K_2qn-青山口组;K_1q-泉头组;K_1d-登娄库组;K_1yc-营城组;K_1sh-沙河子组;K_1h-火石岭组. T03-5:地震层位. 红色区域表示油藏; 五角星代表本文取样点

Fig. 1 Structural units and simple geological map of Northeast China, and structural cross section across the Songliao Basin

(a) a ketch map of main tectonic units; (b) distribution of Paleozoic-Mesozoic magmatic rocks in NE China (modified after Wu *et al.*, 2011; Xu *et al.*, 2013); (c) structural cross section across the central part of the Songliao Basin based on regional seismic analyses. The gray bars in SK1n, SK1s, SK2w and SK2 (or SK2e) are coring intervals and the white bars are un-cored intervals (modified after Wang *et al.*, 2013). The age of Early-Cretaceous mafic rocks from Wang *et al.* (2006b), Zhang *et al.* (2008), Yang *et al.* (2015a), Ying *et al.* (2010), Cui *et al.* (2021), Wu *et al.* (2018) and Pei *et al.* (2008). Abbreviation: XXS-Xinlin-Xiguitu suture; HHS-Heihe-Hegenshan stuture; MYS-Mudanjiang-Yilan suture; SXCYS-Solonker-Xar Moron-Changchun-Yanji suture; JYF-Jiamusi-Yilan fault; DMF-Dunhua-Mishan fault; NT-Nadanhada accretionary terrane; Q-Ey-Quaternary/Neogene; K_2s-Sifangtai Fm.; K_2m-Mingshui Fm.; K_2n-Nenjiang Fm.; K_2y-Yaojia Fm.; K_2qn-Qingshankou Fm.; K_1q-Quantou Fm.; K_1d-Denglouku Fm.; K_1yc-Yingcheng Fm.; K_1sh-Shahezi Fm.; K_1h-Houshigou Fm.. T03-5: seismic horizons. The red regions indicate oil reservoirs. The star represents the location of the collected magmatic samples in this study

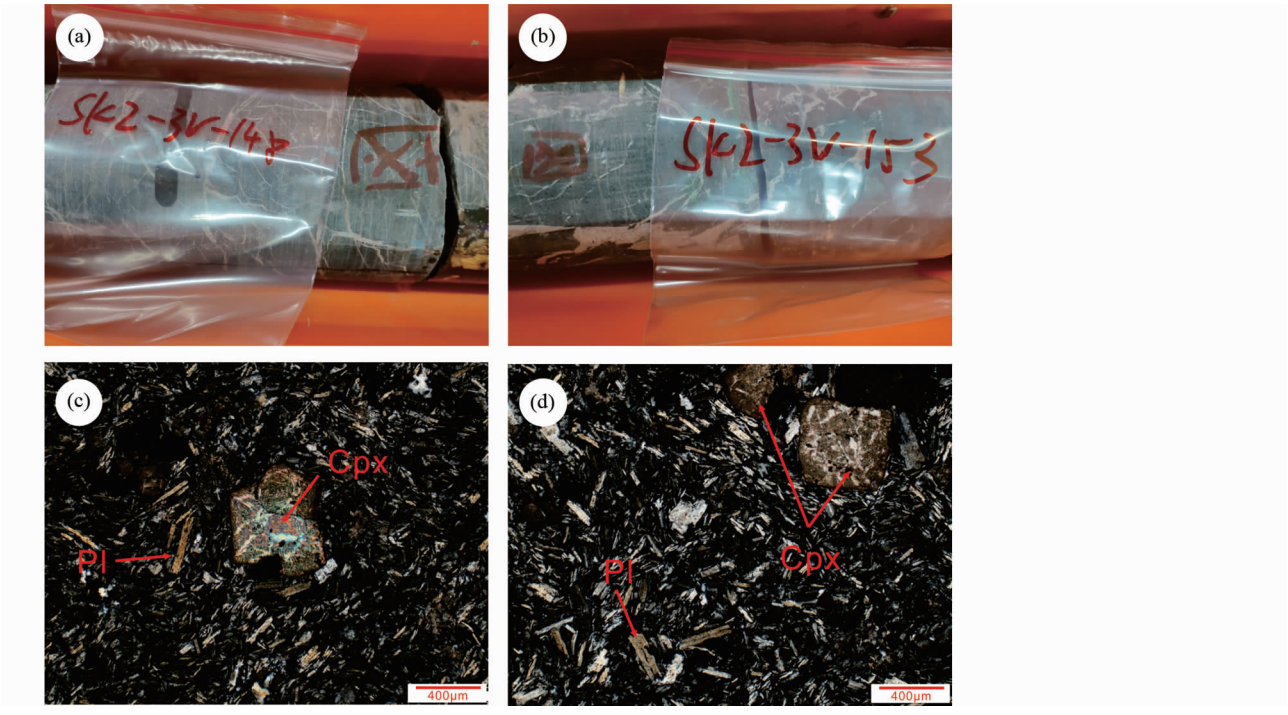

图 2 松科二井样品岩心(a、b)和显微结构(c、d)照片

(a, b)深绿色玄武安山岩岩心,岩心直径约 12cm;(c, d)单斜辉石斑晶与混杂交织的斜长石. Cpx-单斜辉石; Pl-长石

Fig. 2 Core and photomicrographs for the SK2 samples

(a, b) dark green basaltic andesite core, the diameter is about 12cm; (c, d) clinopyroxene phenocrysts and mixed plagioclases. Cpx-clinopyroxene; Pl-plagioclase

松科二井位于位于松辽盆地内的黑龙江省安达市,于 2018 年完钻,其钻井深度达 -7018m,取心层位覆盖营城组、沙河子组、火石岭组等盆地内侏罗系至白垩系地层(侯贺晟等,2018)。本文火山岩样品取自松科二井岩心深 -6035 ~ -6084m,该段岩心呈深绿色,岩性均一为玄武安山岩,部分岩心有大量方解石脉体侵入,受蚀变影响严重(图 2a, b)。通过手标本及镜下观察,本文选择了 9 个新鲜的玄武安山岩样品进行分析,它们均具有斑状结构,斑晶以单斜辉石与斜长石为主,呈半自形,直径为 400 ~ 600μm,含量约为 20vol. %,基质具有典型玻基交织结构,斜长石呈混杂交织状(图 2c, d)。

2 分析方法

将获得的松科二井岩心样品清洗后粉碎至 200 目以下备化学分析。锆石采用常规的重力和磁力法进行分选,将获得的锆石粘贴至环氧树脂靶上,并抛光至露出核部,拍摄透射光、反射光以及阴极发光(CL)照片准备锆石 U-Pb 年龄测试。

锆石 U-Pb 定年测试在中国地质大学(北京)矿物激光微区分析实验室(Milma Lab)通过 LA-ICP-MS 方法完成的。使用连接 Angilent 7900 型 ICP-MS 的 NewWave 193UC 型 ArF 准分子激光器进行剥蚀取样,激光束斑直径 25μm。实验过程中采用锆石 91500 和 NIST 610 作为同位素比值和元素标样,锆石 GJ-1 作为监控标样。数据处理和谐和图绘制分别采用 ICPMSDataCal 和 Isoplot 完成。

全岩主量元素测试在中国科学院地质与地球物理研究所进行,取 200 目样品粉末烘干后称取 0.5g 于陶瓷干锅中,将干锅置于马弗炉中加热至 1000℃,保温 3h。将保温到期

的干锅置于干燥皿中完全冷却后,再次称量其质量,计算得出样品烧失量 LOI。将陶瓷干锅中样品全部取出,添加助熔剂烧制成玻璃片,使用 XRF-1500 X-ray 荧光光谱仪(XRF)完成测试,其精度优于 1% ~3%。

全岩微量元素测试在中国科学院广州地球化学研究所进行,其溶样流程为:(1)准确称取已烘干的 40mg 样品粉末于 Teflon 溶样杯中,加入 0.8mL 1∶1 纯化 HNO_3 与 HF,10 滴 1∶3 $HClO_4$,100℃保温 2 天后,加热蒸干。(2)再次加入 0.8mL 1∶1 纯化 HNO_3 并 100℃保温 12 小时,加入 0.8mL HF 与 10 滴 1∶3 HClO4 密封于高压釜中,190℃加热两天将样品完全溶解。(3)蒸干后再次加入 4N 纯化 HNO_3 密封于高压釜中,170℃加热 4h。(4)将获得溶液用 3% 纯化 HNO_3 稀释定容,定容重量为样品重量的 250 倍。(5)取 0.25g 定容后溶液,以 3% 纯化 HNO_3 稀释至 2.00g,并加入等质量 Rh 内标,准备 ICP-MS 测试。标样 AGV-2、BHVO-2、GSR-1、GSR-2、GSR-3、GSD-9 等与测试样品一同溶解,用于微量校正。样品测试使用 Thermo iCAP Q 电感耦合等离子体质谱仪(ICP-MS),其测试精度优于 5% ~10%。

全岩 Sr-Nd 同位素在广西桂林理工大学广西隐伏金属矿产勘查国家重点实验室完成。根据微量测试获得样品的 Rb、Sr、Sm、Nd 元素含量,分别称取 80 ~120mg 样品于 Teflon 溶样杯中,使用 HF + HNO_3 混合酸 120℃加热溶样一周,通过特效阳离子柱分离 Sr 与 REE,再通过 HDEHP 树脂富集 Nd,使用 Neptune plus MC-ICP-MS 进行测试。$^{143}Nd/^{144}Nd$ 及 $^{86}Sr/^{88}Sr$ 测试结果分别用 $^{146}Nd/^{144}Nd = 0.7129$ 及 $^{86}Sr/^{88}Sr = 0.1194$ 进行标准化,详细测试过程见 Huang *et al.* (2021)和 Chen *et al.* (2013)。

3 分析结果

3.1 锆石 U-Pb 年代学

分选出的锆石粒径约为 50μm,呈透明状扇形或棱柱状。锆石颗粒内部结构均匀,具有板状环带或弱震荡环带,具有较高的 Th、U 含量($Th = 300 \times 10^{-6} \sim 500 \times 10^{-6}$, $U = 2300 \times 10^{-6} \sim 3000 \times 10^{-6}$,表 1)以及高的 Th/U 比值(0.17 ~ 0.59),说明该锆石为岩浆锆石。因岩心样品较少,仅分选出少量锆石,锆石 $^{206}Pb/^{238}U$ 加权平均年龄为 141.6 ± 1.4Ma (1σ, $n = 6$, MSWD = 0.7)(图 3),指示该松科二井该段玄武安山岩形成于早白垩世早期,与前人对火石岭组形成于 140 ~150Ma 的认识相一致(Wang *et al.*, 2002; 瞿雪姣等, 2014)。

3.2 主微量元素

样品的主微量元素组成详见表 2,样品的 SiO_2 含量为 47.32% ~57.24%,$K_2O + Na_2O$ 含量为 3.82% ~6.30%,具有较高的 $Fe_2O_3^T$(6.72% ~ 9.65%)、Al_2O_3(13.7% ~ 16.6%)含量和较低的 CaO(1.77% ~7.59%)含量,其 $Mg^{\#}$

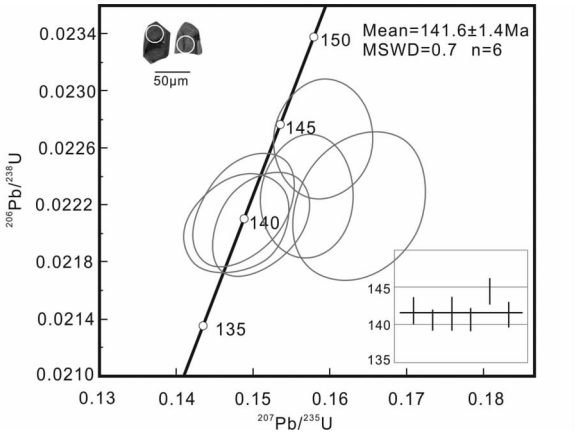

图 3 松科二井玄武安山岩锆石 U-Pb 年龄谐和图与代表性锆石阴极发光图像

Fig. 3 U-Pb concordia diagram with representative cathodoluminescence images of zircons from basaltic andesite in SK2 borehole

值在 53 ~60 之间。在 Nb/Y-Zr/TiO_2 图解中样品主要落入亚碱性玄武岩-安山岩区域(图 4b)。在 Th-Co 图解中样品落入钙碱性玄武岩至玄武安山岩区间内(图 4a)。松辽盆地西侧大兴安岭地区同时代中基性岩石具有更高的 Th 含量,落在高钾钙碱性甚至碱性粗面安山岩范围内,与本文火石岭组玄武安山岩样品具有不同的岩石类型(图 4a)。随 MgO 含量降低,松科二井样品中的 Al_2O_3、CaO、Cr、Ni 含量降低,呈现正相关趋势,而 TiO_2 含量升高,具有负相关趋势(图 5a-f, i)。样品稀土元素总量较低($\Sigma REE = 101 \times 10^{-6} \sim 144 \times 10^{-6}$),且不具有明显的 Eu 异常($\delta Eu = 0.77 \sim 1.56$,平均值 1.01,图 6b);富集轻稀土元素(LREE),相对亏损重稀土元素(HREE),呈现右倾的稀土元素配分模式($(La/Yb)_N = 8.40 \sim 11.88$,图 6b)。在原始地幔标准化微量元素蛛网图中,这些玄武安山岩样品相对富集 Th、U 等大离子亲石元素,轻微亏损 Nb、Ta、Ti 等高场强元素(图 6a)。它们具有与大兴安岭北部根河及南部地区同时代玄武岩相似的稀土元素配分模式,以及具有相似的 Nb、Ta 亏损的特征。但松科二井样品具有更高的 Zr、Hf 与 Ti 含量,以及更高的 Nb/Ta 比值,指示松科二井样品可能与大兴安岭 ~140Ma 玄武岩具有不同的构造背景。

3.3 Sr-Nd 同位素

松科二井样品的 Sr-Nd 同位素数据见表 2,样品的初始 $^{87}Sr/^{86}Sr$ 同位素比值为 0.704956 ~ 0.704802,其初始 $^{143}Nd/^{144}Nd$ 比值为 0.512512 ~ 0.512540,对应的 $\varepsilon_{Nd}(t)$ 值为 1.05 ~ 1.61,其模式年龄为 0.81 ~ 0.88Ga(图 7),与大兴安岭中基性岩的 Sr-Nd 同位素组成相近。

表 1 松科二井玄武安山岩锆石 U-Pb 年龄数据

Table 1 U-Pb age data of zircons from basaltic andesite in SK2 borehole

序号	含量($\times10^{-6}$)			Th/U	同位素比值						年龄(Ma)	
	Pb	Th	U		$^{207}Pb/^{235}U$	1σ	$^{206}Pb/^{238}U$	1σ	$^{207}Pb/^{235}U$	1σ	$^{206}Pb/^{238}U$	1σ
01	73.37	498	2954	0.17	0.1570	0.0040	0.0223	0.0003	148.1	3.5	141.9	1.8
02	58.07	1305	2374	0.55	0.1480	0.0046	0.0221	0.0002	140.2	4.0	140.6	1.4
03	72.58	451	2970	0.15	0.1640	0.0057	0.0222	0.0004	154.2	5.0	141.5	2.2
04	58.79	1434	2424	0.59	0.1509	0.0042	0.0221	0.0002	142.7	3.7	140.7	1.5
05	73.03	1140	2939	0.39	0.1591	0.0043	0.0227	0.0003	149.9	3.8	144.5	1.8
06	56.42	1380	2343	0.59	0.1488	0.0045	0.0222	0.0003	140.8	3.9	141.3	1.7

表 2 松科二井玄武安山岩全岩主量元素(wt%)、微量元素($\times10^{-6}$)和 Sr-Nd 同位素数据

Table 2 Whole-rock major element (wt%), trace element ($\times10^{-6}$) and Sr-Nd isotope data of basaltic andesites from SK2 borehole

样品号	SK2-3V-141	SK2-3V-144	SK2-3V-148	SK2-3V-150	SK2-3V-153	SK2-3V-155	SK2-3V-156	SK2-3V-157	SK2-3V-159
深度(m)	-6035	-6045	-6055	-6062	-6071	-6077	-6080	-6082	-6084
SiO_2	53.5	57.2	51.8	52.4	47.7	47.3	54.5	52.6	54.4
TiO_2	1.17	1.36	1.21	1.22	1.09	1.20	1.36	1.51	1.50
Al_2O_3	15.6	16.0	16.6	16.2	15.3	16.3	13.7	15.0	14.8
$Fe_2O_3^T$	7.97	8.22	6.72	8.09	8.03	7.86	7.37	8.22	9.65
MnO	0.09	0.10	0.11	0.13	0.11	0.12	0.11	0.12	0.10
MgO	4.93	4.93	5.09	6.03	6.27	4.81	4.22	4.68	5.76
CaO	3.84	1.77	5.06	4.56	6.99	7.59	5.95	5.99	4.00
Na_2O	5.35	5.14	5.25	4.41	3.81	3.42	3.06	3.24	1.66
K_2O	1.54	0.71	1.05	1.17	1.22	2.33	1.56	1.73	2.16
P_2O_5	0.38	0.43	0.32	0.32	0.29	0.32	0.38	0.40	0.30
LOI	5.23	4.22	6.24	5.97	8.26	9.03	6.93	7.08	5.36
Total	99.6	100.1	99.4	100.5	99.0	100.3	99.2	100.5	99.8
$Mg^{\#}$	55.1	54.3	60.0	59.6	60.7	54.8	53.1	53.0	54.2
Sc	17.0	14.9	19.7	19.9	18.8	21.0	15.1	15.3	10.3
Ti	7000	8176	7269	7302	6544	7209	8172	9027	8985
V	204	120	130	146	272	327	142	146	142
Cr	367	129	346	309	604	661	111	126	128
Mn	1209	715	889	967	1651	1709	878	894	832
Co	34.7	27.0	31.6	34.5	33.7	37.1	24.9	24.4	30.3
Ni	121.6	81.0	158.3	160.8	153.0	159.3	69.1	68.9	96.5
Cu	15.7	62.3	52.3	48.1	46.4	44.3	35.8	35.6	41.8
Zn	103.8	95.4	90.6	90.6	81.3	87.6	81.7	94.4	102.4
Ga	19.9	20.6	17.3	17.7	15.3	20.5	16.5	18.4	19.3
Ge	2.30	2.19	2.25	2.27	2.26	2.27	2.18	2.17	2.56
Rb	36.3	18.3	24.0	25.0	25.4	110.2	43.8	51.7	20.6
Sr	1005	463	1446	1230	1927	1588	890	993	610
Y	23.6	20.3	18.6	17.9	17.7	19.5	20.1	20.0	16.0
Zr	409	228	206	181	331	350	218	220	222
Nb	9.97	11.48	7.67	7.12	7.06	7.92	12.24	12.63	12.18
Cs	2.34	1.85	2.51	2.34	3.58	5.12	2.65	3.06	3.49
Ba	789	218	769	839	1058	842	408	657	530
La	28.6	22.7	20.0	16.8	18.6	20.1	27.5	20.3	18.6
Ce	113.3	48.4	45.2	38.8	55.4	71.1	58.8	48.7	45.6
Pr	7.92	6.28	5.88	5.12	5.34	5.73	7.26	6.27	6.22

续表 2

Continued Table 2

样品号	SK2-3V-141	SK2-3V-144	SK2-3V-148	SK2-3V-150	SK2-3V-153	SK2-3V-155	SK2-3V-156	SK2-3V-157	SK2-3V-159
深度(m)	-6035	-6045	-6055	-6062	-6071	-6077	-6080	-6082	-6084
Nd	32.2	25.7	24.6	22.6	22.6	24.6	29.9	26.9	25.0
Sm	5.99	4.91	4.87	4.38	4.46	4.84	5.49	5.52	5.32
Eu	1.51	1.49	1.51	1.29	1.36	2.32	1.57	1.29	1.66
Gd	5.35	4.17	4.38	3.95	4.11	4.36	4.82	4.82	4.55
Tb	0.77	0.66	0.64	0.61	0.60	0.64	0.70	0.73	0.73
Dy	4.37	3.75	3.48	3.41	3.26	3.62	3.83	4.14	3.94
Ho	0.87	0.75	0.69	0.65	0.64	0.71	0.76	0.76	0.76
Er	2.23	1.96	1.70	1.73	1.60	1.81	1.88	2.09	1.89
Tm	0.32	0.28	0.25	0.24	0.23	0.25	0.26	0.28	0.28
Yb	2.03	1.80	1.55	1.40	1.44	1.63	1.66	1.68	1.59
Lu	0.31	0.27	0.23	0.22	0.22	0.24	0.25	0.26	0.25
Hf	5.02	5.52	4.66	4.10	3.91	4.43	4.60	4.97	5.09
Ta	0.56	0.69	0.45	0.41	0.40	0.45	0.71	0.77	0.71
Pb	9.24	14.76	5.53	9.74	8.50	9.23	5.89	7.97	8.88
Th	4.57	4.72	3.30	2.98	2.50	2.91	3.18	3.47	1.77
U	1.08	1.97	1.17	0.90	0.78	0.84	0.97	1.00	1.10
$^{87}Rb/^{86}Sr$	0.10		0.20						0.10
$^{87}Sr/^{86}Sr$	0.704990		0.705201						0.705150
1σ	0.000008		0.000008						0.000009
$(^{87}Sr/^{86}Sr)_i$	0.704782		0.704802						0.704956
$^{147}Sm/^{144}Nd$	0.11		0.12						0.13
$^{143}Nd/^{144}Nd$	0.512615		0.512623						0.512658
1σ	0.000004		0.000004						0.000004
$(^{143}Nd/^{144}Nd)_i$	0.512512		0.512514						0.512540
$\varepsilon_{Nd}(t)$	1.05		1.10						1.61
t_{DM}(Ga)	0.80		0.84						0.88

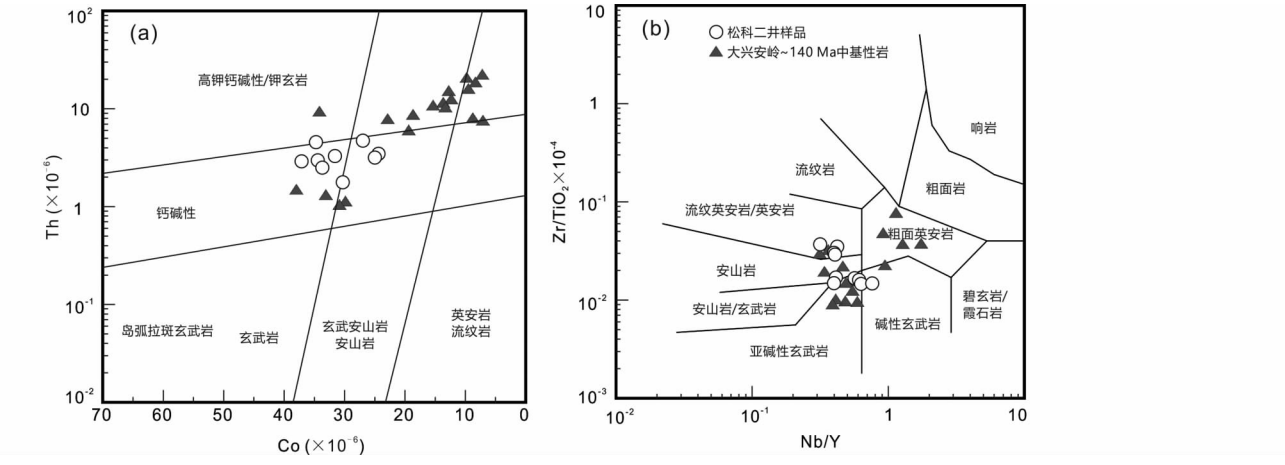

图 4 松科二井玄武安山岩 Th-Co 图解(a, Hastie *et al.*, 2007)及 $Zr/TiO_2 \times 10^{-4}$-Nb/Y 图解(b, Winchester and Floyd, 1977)

本图及图 5-图 8 中大兴安岭~140Ma 中基性岩数据均来源于表 3 所引文献

Fig. 4 Diagrams of Th vs. Co (a, Hastie *et al.*, 2007) and $Zr/TiO_2 \times 10^{-4}$ vs. Nb/Y (b, Winchester and Floyd, 1977) for basaltic andesites from SK2 borehole

The data sources of ~140Ma intermediate to basaltic igneous rocks in the Great Xing'an Range are from Table 3 in this figure and Fig. 5-Fig. 8

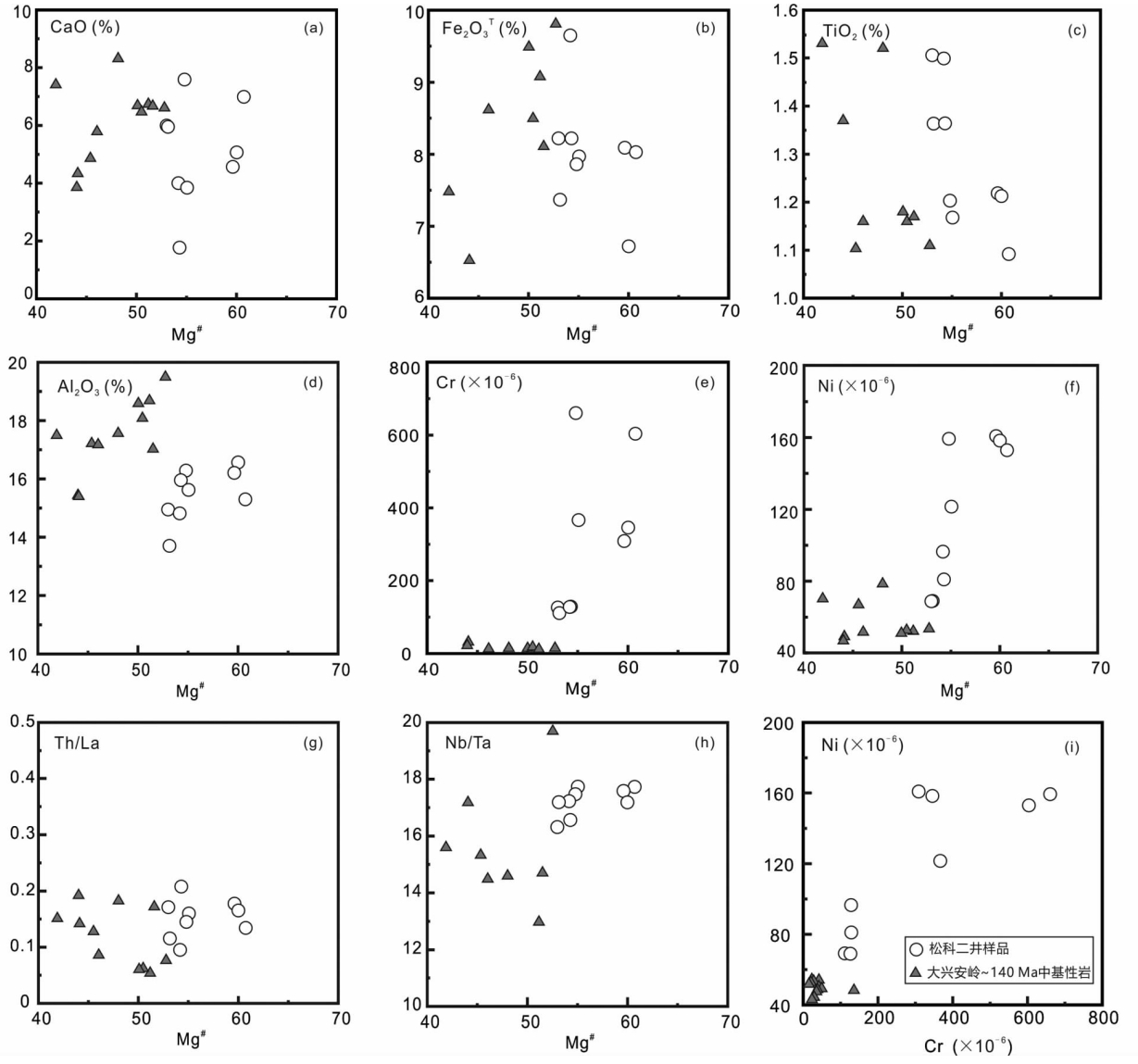

图5 松科二井玄武安山岩及大兴安岭地区同时代中基性岩二元图

Fig. 5 Elemental binary phase diagrams of basaltic andesites in the SK2 borehole and intermediate-basic rocks in the Great Xing'an Range

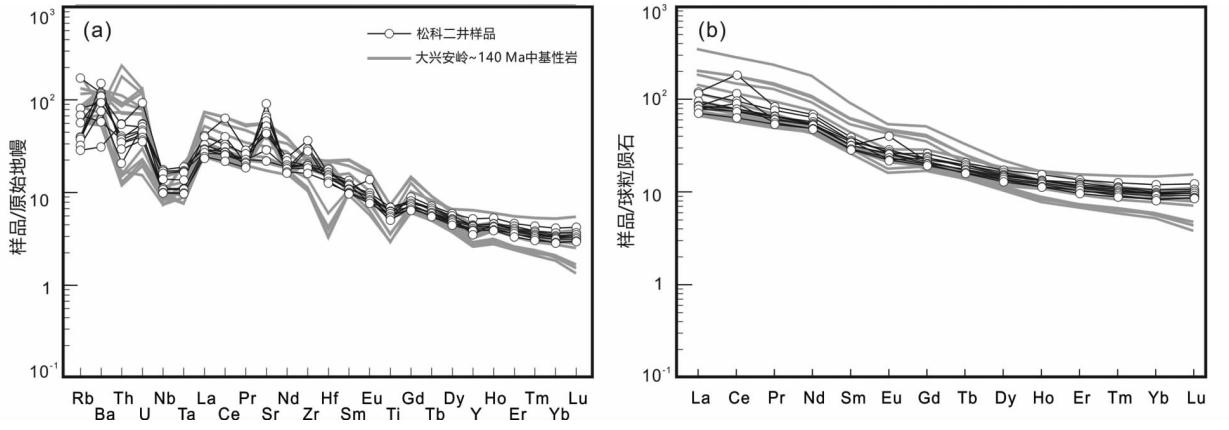

图6 松科二井玄武质安山岩原始地幔标准化微量元素蛛网图(a)和球粒陨石标准化稀土元素配分图(b)(标准化值据 Sun and McDonough, 1989)

Fig. 6 Primitive mantle-normalized trace element spider diagrams (a) and chondrite-normalized REE patterns (b) of basaltic andesites from SK2 borehole (normalization values after Sun and McDonough, 1989)

表 3 早白垩世早期中国东北中基性火山岩年龄

Table 3 Ages of early Early Cretaceous basic-intermediate volcanic rocks in Northeast China

编号	样品号	位置	纬度	经度	岩性	年龄(Ma)	测试方法	参考文献
1	ERBY04-1	满洲里	49°50′32″N	119°57′34″E	玄武岩	140 ± 1	全岩^{40}Ar-^{39}Ar	Wang *et al.* (2006a)
2	ERBY1-9	满洲里	49°50′32″N	119°57′35″E	玄武岩	143 ± 1	全岩^{40}Ar-^{39}Ar	Wang *et al.* (2006a)
3	ERBY04-4	满洲里	49°50′47″N	119°57′37″E	玄武安山岩	140 ± 1	全岩^{40}Ar-^{39}Ar	Wang *et al.* (2006a)
4	GW04037	山河镇	50°26′04″N	120°08′59″E	橄榄玄武岩	139 ± 1.8	全岩^{40}Ar-^{39}Ar	Zhang *et al.* (2008)
5	GW04037	山河镇	50°26′04″N	120°08′59″E	橄榄玄武岩	139 ± 2	锆石 LA-ICP-MS	Zhang *et al.* (2008)
6	D2556	奇力滨林场	—	—	安山岩	141 ± 1.2	锆石 LA-ICP-MS	崔玉斌等(2021)
7	PM05-3TW1	奇力滨林场	—	—	安山岩	142 ± 3	锆石 LA-ICP-MS	崔玉斌等(2021)
8	D1059	根河	50°33′14″N	121°22′54″E	玄武安山岩	142 ± 2.1	锆石 LA-ICP-MS	吴涛涛等(2018)
9	TW4	突泉	45°32′19″N	121°10′57″E	粗面岩	138 ± 2	锆石 LA-ICP-MS	Yang *et al.* (2015a)
10	TW9	突泉	45°37′57″N	121°22′54″E	粗面岩	142 ± 3	锆石 LA-ICP-MS	Yang *et al.* (2015a)
11	TQBS04-2	突泉	46°02′40″N	121°07′22″E	安山岩	140 ± 1	锆石 LA-ICP-MS	Ying *et al.* (2010)
12	SN190-12	火石岭组	44°55′00″N	123°24′43″E	粗面安山岩	133 ± 1	锆石 LA-ICP-MS	裴福萍等(2008)
13	PK10-6	火石岭组	43°53′31″N	124°14′49″E	粗面安山岩	129 ± 2	锆石 LA-ICP-MS	裴福萍等(2008)
14	D069	玛尼土组	44°38′18″N	112°23′40″E	粗面安山岩	140.5 ± 2	锆石 LA-ICP-MS	Zhang *et al.* (2017)
15	D002	玛尼土组	44°37′17″N	112°18′45″E	粗面安山岩	138.9 ± 2	锆石 LA-ICP-MS	Zhang *et al.* (2017)
16	EGN32	穆瑞农场	49°53′16″N	121°17′43″E	玄武岩	138.5 ± 2.2	全岩 K-Ar	Fan *et al.* (2003)

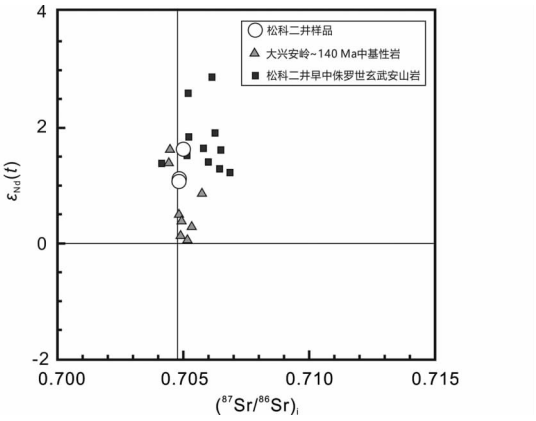

图 7 松科二井玄武安山岩 $\varepsilon_{Nd}(t)$-$(^{87}Sr/^{86}Sr)_i$ 协变图

松科二井早中侏罗世玄武安山岩 Sr-Nd 同位素数据引自 Huang *et al.* (2021)

Fig. 7 $\varepsilon_{Nd}(t)$ vs. $(^{87}Sr/^{86}Sr)_i$ diagram of basaltic andesites in SK2 borehole

Data of Early Middle Jurassic basaltic andesites in SK2 borehole from Huang *et al.* (2021)

4 讨论

4.1 东北早白垩世火山岩分布

本文系统总结了中国东北已有的早白垩世早期中基性火山岩的年代学数据(表 3),大兴安岭地区早白垩世早期火山岩发育于大兴安岭北部玛尼土组及大兴安岭南部塔木兰沟组火山岩地层中(Wang *et al.*, 2006b; Ying *et al.*, 2010),与大规模出露的花岗岩相比,中基性岩的报道较为有限。大兴安岭北部早白垩世中基性岩沿满洲里至根河分布于大兴安岭西缘,Wang *et al.* (2006a)使用^{40}Ar-^{39}Ar 法获得大兴安岭北部满洲里地区玄武岩锆石年龄为 143 ~ 140Ma;Zhang *et al.* (2008)使用^{40}Ar-^{39}Ar 与 LA-ICP-MS 测试大兴安岭北部山河镇地区塔木兰沟组橄榄玄武岩,获得了一致的年龄为 139Ma;崔玉斌等(2021)与吴涛涛等(2018)在根河及其附近的奇力滨林场地区获得了玛尼土组 141 ~ 140Ma 的安山岩与玄武安山岩。大兴安岭南部地区早白垩世早期火山岩主要发育于靠近松辽盆地西缘的突泉等地,其锆石 U-Pb 年龄为 142 ~ 138Ma,属于塔木兰沟组与玛尼土组(Zhang *et al.* 2008; Ying *et al.*, 2010; Yang *et al.*, 2015a)。

松辽盆地早白垩世火山岩以中酸性岩为主,其年龄集中于 120 ~ 100Ma 的营城组中。早白垩世早期火山岩罕有报导,裴福萍等(2008)在盆地西部松南 190 井获得的火石岭组粗面安山岩锆石 U-Pb 年龄为 133 ~ 129Ma,是目前松辽盆地北部发现的最老的白垩纪火山岩年龄。对区域上已有岩浆岩的时空分布研究显示,在松辽盆地以及黑龙江-吉林东部地区可能存在晚侏罗世(~160Ma)持续至早白垩世早期(~130Ma)的岩浆间歇期(Ji *et al.*, 2019b; Wu *et al.*, 2019; Ma and Xu, 2021)。因此早白垩世早期岩浆作用主要集中于松辽盆地以西。本文获得松辽盆地火石岭组玄武安山岩形成时代为 141.6 ± 1.4Ma,反映了早白垩世早期岩浆活动很可能蔓延至松辽盆地内部。

4.2 岩石成因

源自岩石圈深部的基性岩浆形成后喷发至地表过程中需经过较厚的大陆地壳,地壳物质可能混染岩浆组成,使用这些岩浆化学成分反演源区组成前需剔除可能的地壳混染过程。相对于地幔熔体,地壳物质通常具有较低的 Nb、Ta 含量、较高的 Th 含量,和较低的 Nb/Ta 比值(8.33 ~ 13.33, Hofmann, 1988),地壳混染会导致熔体中 Nb/Ta 比值下降,Th/La 比值上升。本文松科二井火山岩样品的 Nb/Ta 比值在 16.2 ~ 17.7 之间,平均值 17.2,更接近于地幔熔体(如 N-MORB,$Ta = 0.192 \times 10^{-6}$,$Nb = 3.507 \times 10^{-6}$,Nb/Ta = 18.27; Hofmann, 1988)。样品 Nb/Ta 和 Th/La 比值与 $Mg^{\#}$之间未呈现任何趋势(Cao *et al.*, 2019, 图 5g-h)说明在松科二井玄武安山岩形成过程中,未受明显地壳混染。相比于原始岩浆,地壳混染后的岩浆具有较高的 Th/Nb (>5),Th/Ta 值(>10)(Wooden *et al.*, 1993; Neal *et al.*, 2002),而松科二井样品的 Th/Nb 值(0.15 ~ 0.46)与 Th/Ta 值(2.50 ~ 8.13)均较低,没有表现出地壳混染的特征。因而,松科二井玄武安山岩样品的地球化学特征可以反映其地幔源区的特征。

松科二井玄武安山岩样品 $Mg^{\#}$值介于 53 ~ 60 之间,略小于地幔 $Mg^{\#}$值(68 ~ 75; Neal *et al.*, 2002),Ni 含量($68 \times 10^{-6} \sim 160 \times 10^{-6}$)较低,说明岩浆经历过镁铁质矿物的分离结晶作用。如图 5 中所示,Cr-Ni 呈现明显的正相关性,$Mg^{\#}$与 CaO、Al_2O_3、Cr、Ni 均具显示正相关关系,而与 TiO_2 具有负相关性,说明岩浆演化早期可能有橄榄石和单斜辉石等镁铁矿物分离结晶。根据 100(Fe + Mg + Mn)/Ti-100Si/Ti 图解(图 8),松科二井玄武安山岩样品数据分布于单斜辉石分离结晶线附近,同样说明岩浆演化过程中发生了以单斜辉石为主的分离结晶作用。在球粒陨石标准化稀土元素配分图中(图 6b)没有显示出 Eu 与 Sr 的负异常,说明长石未发生分离结晶。

松科二井样品显示了明显富集大离子亲石元素和亏损高场强元素,为典型的弧岩浆特征。在排除地壳混染的影响后,其 Nb、Ta 亏损特征很可能继承自源区,指示其源区岩石圈地幔受到了俯冲作用的改造。俯冲板片熔融的熔体更富集 Th 等高场强元素,若样品受到了熔体改造,其高场强元素的变化范围较大。本文样品具有变化范围较小的 Th/Nd 比值(0.07 ~ 0.18),Zr/Nd 比值(7.32 ~ 14.65),且在稀土元素配分图上(图 6b),HREE 较为平缓,说明样品未受俯冲熔体的改造,相对富集的大离子亲石元素含量可能受到了俯冲过程中板片流体的改造。

板片脱水流体对岩浆中活动性强的大离子亲石元素影响较大,而对流体活动性弱的稀土元素和高场强元素基本没有影响,因此可以使用 La,Sm, Nd 和 Yb 等稀土元素对地幔熔融程度和源区组成进行反演(Xu *et al.* 2000; Huang *et al.*, 2017, 2021)。由于 Yb 等重稀土元素易于进入石榴石中,而轻中稀土元素 La,Sm 等在石榴石中含量较低,石榴石

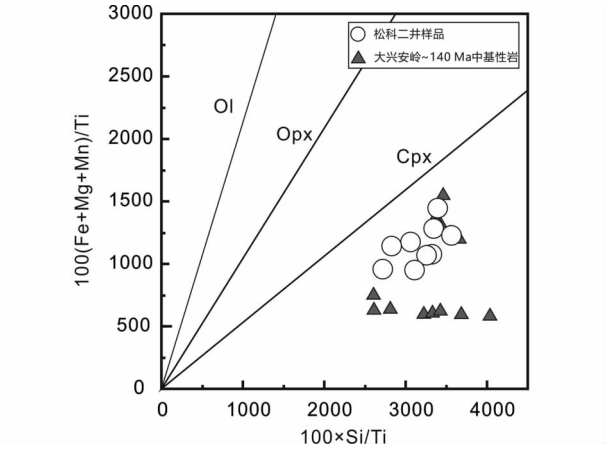

图 8 松科二井玄武安山岩 100(Fe + Mg + Mn)/Ti-100 × Si/Ti 图解

Ol、Opx 和 Cpx 分别代表橄榄石、斜方辉石和单斜辉石分离的结晶趋势

Fig. 8 100(Fe + Mg + Mn)/Ti vs. 100 × Si/Ti diagram of basaltic andesites in SK2 borehole

Ol, Opx and Cpx represent fractional crystallization trend of olivine, Opx and Cpx, respectively

的熔融能够显著改变初始岩浆 Sm/Yb 比值,而在尖晶石稳定相中,La/Sm 比值基本保持不变。在 Sm/Yb-La/Sm 图解(图 9;Aldanmaz *et al.*, 2000),松科二井玄武安山岩样品位于石榴石:尖晶石 = 1:1 源区批式部分熔融的曲线上,显示其初始岩浆可能为地幔中石榴石-尖晶石相变带经低程度部分熔融产生。松科二井玄武安山岩的 Sr-Nd 同位素特征($(^{87}Sr/^{86}Sr)_i = 0.704802 \sim 0.704956$,$\varepsilon_{Nd}(t) = 1.05 \sim 1.61$)与松科二井内早侏罗世玄武岩的同位素特征相近(图 7),表明自侏罗纪以来,松辽盆地下部岩石圈地幔并未受到明显的同位素改造。因此,松科二井早白垩世早期玄武安山岩可能是较浅的石榴石-尖晶石相转变带经低程度部分熔融形成。

4.3 构造动力学意义

中国东北地区中生代构造演化受古亚洲洋、蒙古-鄂霍茨克构造域与环太平洋构造域影响(Xu *et al.*, 2009)。已有研究显示,古亚洲洋关闭于早-中三叠世前(Wang *et al.*, 2018; Li *et al.*, 2020),中生代末期中国东北主要受控于蒙古-鄂霍茨克洋与古太平洋的俯冲或闭合作用影响,然而目前对两大构造域的影响范围尚无统一认识。侏罗纪以来,蒙古-鄂霍茨克洋始终向北俯冲至西伯利亚克拉通之下,在早白垩世(Sorokin *et al.*, 2003)或晚白垩世开始南北双向俯冲(Chen *et al.*, 2011; Li *et al.*, 2020),并在东北北部和中部诱发形成了碱性-钙碱性岩浆作用(Xu *et al.*, 2013; Li *et al.*, 2018)。Smirnova *et al.* (2017)认为蒙古-鄂霍茨克洋关闭于早-中侏罗世,而 Yang *et al.* (2015b)认为在早白垩世时期,蒙古-鄂霍茨克洋的主体已经关闭,但在漠河以北仍有残留

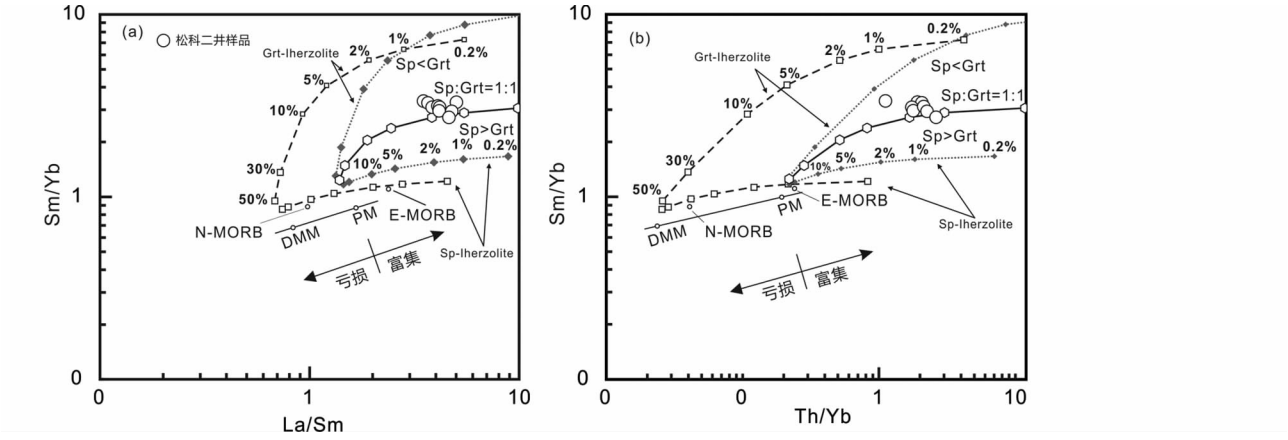

图 9 松科二井玄武安山岩 La/Sm-Sm/Yb(a)与 Th/Yb-Sm/Yb(b)图解

两图中曲线表示尖晶石二辉橄榄岩和石榴石二辉橄榄岩的平衡部分熔融曲线. 源区与熔体的矿物比例根据 Aldanmaz *et al.* (2000). 矿物/基质分配系数来自 Mckenzie and Onions(1991); DMM 成分引自 Workman and Hart (2005); PM、N-MORB and E-MORB 成分根据 Sun and McDonough (1989). 带有空心方块的和实心方块的曲线分别是 DMM 和 PM 的熔融趋势线. 带正六边形的实线代表 50% 尖晶石二辉橄榄岩和 50% 石榴石二辉橄榄岩的混合熔体, 每条曲线上的百分比等于对应地幔源区的部分熔融程度

Fig. 9 Plots of La/Sm vs. Sm/Yb (a) and Th/Yb vs. Sm/Yb (b) of basaltic andesites from SK2 borehole showing melt curves obtained using the non-modal batch melting

Melt curves are drawn for spinel-lherzolite and for garnet lherzolite, mineral proportion of the sources and melts after Aldanmaz *et al.* (2000). Mineral/matrix partition coefficients are from Mckenzie and Onions (1991). DMM composition is from Workman and Hart (2005); PM, N-MORB and E-MORB compositions are from Sun and McDonough (1989). The line with empty square and filled square represent the melting trends from DMM and PM, respectively; the solid line with regular hexagon represents the hybrid melts from 50% spinel-lherzolite and 50% garnet-lherzolite. The percentages on each curve correspond to degrees of partial melting for a given mantle source

洋盆(Parfenov *et al.*, 2010; Yang *et al.*, 2015b),蒙古-鄂霍茨克洋关闭于晚侏罗至早白垩世(155 ~ 135Ma)。因此,蒙古-鄂霍茨克洋的影响时代与范围覆盖了松辽盆地形成和演化的时期(侏罗至白垩纪),Zhang *et al.* (2017)认为大兴安岭南部 140Ma 玄武岩形成于蒙古-鄂霍茨克洋盆关闭后的岩石圈伸展构造环境,但蒙古-鄂霍茨克洋板片南向俯冲是否影响了松辽盆地的形成和演化尚不清楚。本文报道的松科二井盆地内部的早白垩世火山岩显示了与盆地早侏罗世玄武安山岩及盆地西侧大兴安岭地区类似的 Sr-Nd 同位素组成(图 7),但是具有明显不同的岩石组合和主量元素特征(图 4、图 5),表明它们很可能未受到蒙古-鄂霍茨克洋俯冲和闭合过程的影响。

对于环太平洋构造域,位于东北地区东部的佳木斯地块东缘早侏罗世钙碱性火山岩及中部的松辽盆地内双峰式火山岩指示它们分别对应活动大陆边缘和弧后伸展背景,共同指示东侧古太平洋俯冲始于早侏罗世(Wu *et al.*, 2007; Tang *et al.*, 2018; Wang *et al.*, 2019)。松辽盆地西侧出现大量中-晚侏罗世至早白垩世早期岩浆作用,表明古太平洋板块持续往东北内部俯冲(Tang *et al.*, 2018)。Ji *et al.* (2019b)通过收集整理中国东北地区侏罗至白垩纪火山岩的年龄数据,发现侏罗纪至早白垩世期间,中国东北地区的火山活动呈现出时空上的迁移特征:(1)侏罗纪(200 ~ 145Ma)期间从黑龙江-吉林省东部至松辽盆地西缘火山岩由老至新;(2)白垩纪(145 ~ 80Ma)期间由松辽盆地西缘至黑龙江-吉林省东部火山岩年龄逐渐年轻;(3)松辽盆地及黑龙江-吉林东部在晚侏罗世至早白垩世期间存在较长时间的岩浆间歇期(ca. 160 ~ 135Ma)。Ma and Xu (2021)及 Wu *et al.* (2019)也发现了这一特征,他们认为在 ~ 145Ma 的时期古太平洋板片由东向西低角度俯冲转变为板片后撤回转是导致岩浆活动迁移的主要原因。松辽盆地内早白垩世晚期(120 ~ 100Ma)广泛发育的 A 型流纹岩及埃达克质岩同样暗示早白垩世时期盆地处于拉张环境(Yang *et al.* 2015a), Ji *et al.* (2019a)认为埃达克质岩与 A 型流纹岩成因与古太平洋板片后撤回转导致的拆沉作用与地幔上涌相关。Ji *et al.* (2019b)通过对比在海拉尔盆地出露的 145Ma 的高钾与低钾两种不同埃达克质岩的成因,提出古太平洋俯冲至少抵达了松辽盆地以西的海拉尔盆地。因此,松辽盆地晚侏罗世至早白垩世的构造演化应主要受古太平洋构造域的影响,但由于盆地内早白垩世早期火山岩极少出露,古太平洋俯冲与回转对盆地演化的影响尚不明确。

本文样品具有与板内玄武岩相近的 Hf/Th 比值(1.10 ~ 2.87)与 Th/Nb 比值(0.15 ~ 0.46) (Hf/Th < 8, Th/Nb > 0.11),具有较高的 Zr 含量($206 \times 10^{-6} \sim 409 \times 10^{-6}$)及 Zr/Y 比值(10.13 ~ 18.69),并在 Zr/Y-Zr 构造判别图解上落于板内玄武岩区域上方(图 10a),在 Zr/Y-Ti/Y 图解上位于板内玄武岩区域(图 10b),在 Th/Hf-Ta/Hf 图解中落于陆内裂谷玄武岩区域(图 10c),指示松科二井早白垩世玄武安山岩形成于板内环境,这与蒙古-鄂霍茨克洋南向俯冲及古太平洋

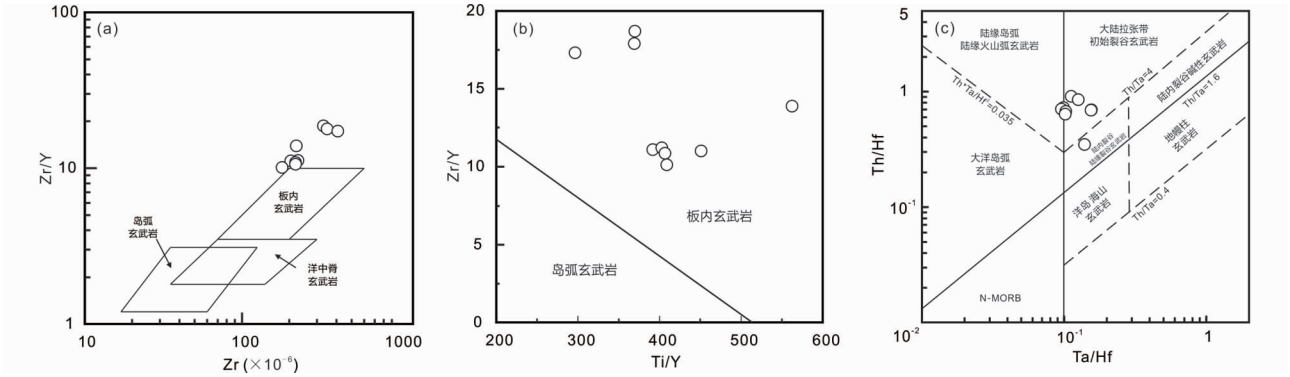

图 10 松科二井玄武安山岩的构造判别图解

(a) Zr/Y-Zr (Pearce and Norry,1979); (b) Zr/Y -Ti/Y 图解 (Pearce and Gale, 1977); (c) Th/Hf-Ta/Hf 判别图解 (汪云亮等,2001)

Fig. 10 Plots of tectonic discrimination of basaltic andesites from SK2 borehole

(a) Zr/Y vs. Zr (Pearce and Norry,1979); (b) Zr/Y vs. Ti/Y (Pearce and Gale, 1977); (c) Th/Hf vs. Ta/Hf (Wang *et al.*, 2001)

西向俯冲产生的大量弧岩浆明显不同。可能指示早白垩世早期松辽盆地玄武安山岩的形成与蒙古-鄂霍茨克洋南向俯冲及古太平洋低角度俯冲并非直接相关,主要受控于古太平洋板片俯冲回转过程。

古太平洋初始俯冲诱发的岩石圈伸展可能引发了松科二井中侏罗世早期的玄武质岩浆作用,并导致了盆地雏形的形成(Huang *et al.*, 2021),中侏罗世至晚侏罗世时期古太平洋持续西向低角度俯冲,导致中国东北岩浆活动由黑龙江-吉林东部向西迁移至大兴安岭西缘,其俯冲过程可能一定程度上改造了松辽盆地岩石圈地幔。在早白垩世早期,古太平洋板片回转导致的地幔上涌加热了浅部岩石圈地幔,并促使其发生低程度部分熔融,形成早白垩世早期玄武安山岩,而地幔上涌引发的岩石圈减薄则影响了松辽盆地早期沉降,从而形成了早白垩世时期大量火石岭组、沙河子组及营城组沉积岩。

5 结论

(1)锆石 U-Pb 定年揭示松科二井火石岭组玄武安山岩形成于早白垩世早期,其年龄为 141.6 ± 1.4Ma,暗示松辽盆地内早白垩世火山活动始于 ~140Ma。

(2)松科二井玄武安山岩具有轻微亏损的 Sr-Nd 同位素特征,起源于较浅的石榴石-尖晶石地幔相变带低程度部分熔融。

(3)松科二井玄武安山岩具有板内玄武岩的地球化学特征,可能暗示其形成于古太平洋板片回转导致的地幔上涌,指示松辽盆地早期演化主要受控于古太平洋板片回转引发的地幔上涌与岩石圈减薄。

致谢 感谢两位匿名审稿人提出的宝贵建议;感谢薛丁帅、孙胜玲、涂湘林、张银慧、余红霞和张亮亮老师在锆石定年和全岩化学分析过程中提供的帮助;感谢范子尘,杨昌琦,陈钦和李明键同学在岩心取样和样品处理过程中提供的帮助。

References

Aldanmaz E, Pearce JA, Thirlwall MF and Mitchell JG. 2000. Petrogenetic evolution of Late Cenozoic, post-collision volcanism in western Anatolia, Turkey. Journal of Volcanology and Geothermal Research, 102(1-2): 67-95

Cao K, Yang ZM, Xu JF, Fu B, Li WK and Sun MY. 2019. Origin of dioritic magma and its contribution to porphyry Cu-Au mineralization at Pulang in the Yidun arc, eastern Tibet. Lithos, 304-307: 436-449

Chang WB, Shan XL, Yi J, Du TT and Qu Y. 2017. Spatial and temporal distributions of the Late Mesozoic volcanic successions and their controlling effects on the Changling fault depression of the Songliao Basin, Northeast China. Canadian Journal of Earth Sciences, 54(12): 1194-1213

Chen JL, Wu JB, Xu JF, Dong YH, Wang BD and Kang ZQ. 2013. Geochemistry of Eocene high-Mg# adakitic rocks in the northern Qiangtang terrane, central Tibet: Implications for early uplift of the plateau. Geological Society of America Bulletin, 125(11-12): 1800-1819

Chen PJ and Chang ZL. 1994. Nonmarine Cretaceous stratigraphy of eastern China. Cretaceous Research, 15(3): 245-257

Chen ZG, Zhang LC, Wan B, Wu HY and Cleven N. 2011. Geochronology and geochemistry of the Wunugetushan porphyry Cu-Mo deposit in NE China, and their geological significance. Ore Geology Reviews, 43(1): 92-105

Cui YB, Wang K, He FB, Yin GW, Wang ZL, Wang GL and She SK. 2021. Geochronology and geochemical characteristics of volcanic rocks from the Manitu Formation in the Qilibin area, northern Great Xing'an Range and its geological significance. Acta Geologica Sinica, 95(11): 3301-3316 (in Chinese with English abstract)

Fan WM, Guo F, Wang YJ and Lin G. 2003. Late Mesozoic calc-alkaline volcanism of post-orogenic extension in the northern Da Hinggan Mountains, northeastern China. Journal of Volcanology and Geothermal Research, 121(1-2): 115-135

Ge WC, Sui ZM, Wu FY, Zhang JH, Xu XC and Cheng RY. 2007. Zircon U-Pb ages, Hf isotopic characteristics and their implications of the Early Paleozoic granites in the northeastern Da Hinggan Mts, northeastern China. Acta Petrologica Sinica, 23(2): 423-440 (in

Chinese with English abstract)
Hastie AR, Kerr AC, Pearce JA and Mitchell SF. 2007. Classification of altered volcanic island arc rocks using immobile trace elements: Development of the Th-Co discrimination diagram. Journal of Petrology, 48(12): 2341 – 2357
Hofmann AW. 1988. Chemical differentiation of the Earth: The relationship between mantle, continental crust, and oceanic crust. Earth and Planetary Science Letters, 90(3): 297 – 314
Hou HS, Wang CS, Zhang JD, Ma F, Fu W, Wang PJ, Huang YJ, Zou CC, Gao YF, Gao Y, Zhang LM, Yang J and Guo R. 2018. Deep continental scientific drilling engineering in Songliao Basin: Progress in earth science research. Geology in China, 45(4): 641 – 657 (in Chinese with English abstract)
Huang F, Xu JF, Liu YS, Li J, Chen JL and Li XY. 2017. Re-Os isotope evidence from Mesozoic and Cenozoic basalts for secular evolution of the mantle beneath the North China Craton. Contributions to Mineralogy and Petrology, 172(5): 28
Huang F, Zhang Z, Xu JF, Li XY, Zeng YC, Xu R, Liu XJ, Zhang LY, Zhang M, Yang CQ, Zhang LL, Yu HX and Yang XL. 2021. Lithospheric extension in response to subduction of the Paleo-Pacific Plate: Insights from Early Jurassic intraplate volcanic rocks in the Sk2 Borehole, Songliao Basin, NE China. Lithos, 380 – 381: 1058714
Ji Z, Meng QA, Wan CB, Ge WC, Yang H, Zhang YL, Dong Y and Jin X. 2019a. Early Cretaceous adakitic lavas and A-type rhyolites in the Songliao Basin, NE China: Implications for the mechanism of lithospheric extension. Gondwana Research, 71: 28 – 48
Ji Z, Meng QA, Wan CB, Zhu DF, Ge WC, Zhang YL, Yang H and Dong Y. 2019b. Geodynamic evolution of flat-slab subduction of Paleo-Pacific Plate: Constraints from Jurassic adakitic lavas in the Hailar Basin, NE China. Tectonics, 38(12): 4301 – 4319
Li JY. 2006. Permian geodynamic setting of Northeast China and adjacent regions: Closure of the Paleo-Asian Ocean and subduction of the Paleo-Pacific Plate. Journal of Asian Earth Sciences, 26(3 – 4): 207 – 224
Li SQ, Wang Y, Fang BW, He JF, Chen FK and Siebel W. 2019. Early Cretaceous rift-related volcanism in the Songliao Basin, NE China: A geochemical study. International Geology Review, 61(1): 39 – 55
Li Y, Xu WL, Wang F, Tang J, Pei FP and Wang ZJ. 2014. Geochronology and geochemistry of Late Paleozoic volcanic rocks on the western margin of the Songnen-Zhangguangcai Range Massif, NE China: Implications for the amalgamation history of the Xing'an and Songnen-Zhangguangcai Range massifs. Lithos, 205: 394 – 410
Li Y, Xu WL, Tang J, Pei FP, Wang F and Sun CY. 2018. Geochronology and geochemistry of Mesozoic intrusive rocks in the Xing'an Massif of NE China: Implications for the evolution and spatial extent of the Mongol-Okhotsk tectonic regime. Lithos, 304 – 307: 57 – 73
Li Y, Xu WL, Zhu RX, Wang F, Ge WC and Sorokin AA. 2020. Late Jurassic to early Early Cretaceous tectonic nature on the NE Asian continental margin: Constraints from Mesozoic accretionary complexes. Earth-Science Reviews, 200: 103042
Li ZQ, Chen JL, Zou H, Wang CS, Meng QA, Liu HL and Wang SZ. 2021. Mesozoic-Cenozoic tectonic evolution and dynamics of the Songliao Basin, NE Asia: Implications for the closure of the Paleo-Asian Ocean and Mongol-Okhotsk Ocean and subduction of the Paleo-Pacific Ocean. Earth-Science Reviews, 218: 103471
Liu YJ, Li WM, Feng ZQ, Wen QB, Neubauer F and Liang CY. 2017. A review of the Paleozoic tectonics in the eastern part of Central Asian Orogenic Belt. Gondwana Research, 43: 123 – 148
Ma Q and Xu YG. 2021. Magmatic perspective on subduction of Paleo-Pacific Plate and initiation of big mantle wedge in East Asia. Earth-Science Reviews, 213: 103473
Mckenzie D and Onions RK. 1991. Partial melt distributions from inversion of rare-earth element concentrations. Journal of Petrology, 32: 1021 – 1091
Miao LC, Zhang FC and Jiao SJ. 2015. Age, protoliths and tectonic implications of the Toudaoqiao blueschist, Inner Mongolia, China. Journal of Asian Earth Sciences, 105: 360 – 373
Neal CR, Mahoney JJ and Chazey WJ. 2002. Mantle sources and the highly variable role of continental lithosphere in basalt petrogenesis of the Kerguelen Plateau and Broken Ridge LIP: Results from ODP Leg 183. Journal of Petrology, 43(7): 1177 – 1205
Parfenov LM, Berzin NA, Badarch G, Belichenko VG, Bulgatov AN, Dril SI, Khanchuk AI, Kirillova GL, Kuz'min MI, Nokleberg WJ, Ogasawara M, Obolenskiy AA, Prokopiev AV, Rodionov SM, Scotese CR, Timofeev VF, Tomurtogoo O and Yan HQ. 2010. Tectonic and metallogenic model for Northeast Asia. In: Nokleberg WJ (ed.). Metallogenesis and Tectonics of Northeast Asia. U. S. Geological Survey Professional Paper, 1765
Pearce JA and Gale GH. 1977. Identification of ore-deposition environment from trace element geochemistry of associated igneous host rocks. Geological Society of London, Special Publication, 7: 14 – 24
Pearce JA and Norry MJ. 1979. Petrogenetic implications of Ti, Zr, Y and Nb variations in volcanic rocks. Contributions to Mineralogy and Petrology, 69: 33 – 47
Pei FP, Xu WL, Yang DB, Ji WQ, Yu Y and Zhang XZ. 2008. Mesozoic volcanic rocks in the southern Songliao Basin: Zircon U-Pb ages and their constraints on the nature of basin basement. Earth Science, 33(5): 603 – 617 (in Chinese with English abstract)
Qu XJ, Wang PJ, Gao YF and Wan XQ. 2014. Chronostratigraphy of Huoshiling Formation in the Songliao Basin, NE China: An overview. Earth Science Frontiers, 21(2): 234 – 250 (in Chinese with English abstract)
Smirnova YN, Sorokin AA, Popeko LI, Kotov AB and Kovach VP. 2017. Geochemistry and provenances of the Jurassic Terrigenous rocks of the Upper Amur and Zeya-Dep troughs, eastern Central Asian fold belt. Geochemistry International, 55(2): 163 – 183
Sorokin AA, Kudryashov NM, Sorokin AP, Rublev AG, Levchenkov OA, Kotov AB, Sal'nikova EB and Kovach VP. 2003. Geochronology, geochemistry, and geodynamic setting of Paleozoic granitoids in the eastern segment of Mongol-Okhotsk belt. Doklady Earth Sciences, 393(8): 1136 – 1140
Sun SS and McDonough WF. 1989. Chemical and isotopic systematics of oceanic basalts: Implications for mantle composition and processes. In: Saunders AD and Norry MJ (eds.). Magmatism in the Ocean Basins. Geological Society, London, Special Publications, 42(1): 313 – 345
Tang J, Xu WL, Wang F and Ge WC. 2018. Subduction history of the Paleo-Pacific slab beneath Eurasian continent: Mesozoic-Paleogene magmatic records in Northeast Asia. Science China (Earth Sciences), 61(5): 527 – 559
Wang CL, Zhang MS, Sun K, Wang YN, Li XB and Liu XS. 2017. Latest zircon U-Pb geochronology of the Huoshiling Formation volcanic rocks in the southeastern margin of the Songliao Basin. Acta Geologica Sinica (English Edition), 91(5): 1924 – 1925
Wang CM, Zhu JX, Bagas L, Chen Q, Zhang ZC, Duan HY and Liu LJ. 2022. Whether short-lived or prolonged duration of multistage combined magmatic and hydrothermal events in the giant Chalukou porphyry Mo deposit, China. Ore Geology Reviews, 140: 104576
Wang CS, Feng ZQ, Zhang LM, Huang YJ, Cao K, Wang PJ and Zhao B. 2013. Cretaceous paleogeography and paleoclimate and the setting of SKI borehole sites in Songliao Basin, Northeast China. Palaeogeography, Palaeoclimatology, Palaeoecology, 385: 17 – 30
Wang F, Zhou XH, Zhang LC, Ying JF, Zhang YT, Wu FY and Zhu RX. 2006b. Late Mesozoic volcanism in the Great Xing'an range (NE China): Timing and implications for the dynamic setting of NE Asia. Earth and Planetary Science Letters, 251(1 – 2): 179 – 198
Wang F, Xu WL, Meng E, Cao HH and Gao FH. 2012. Early Paleozoic amalgamation of the Songnen-Zhangguangcai Range and Jiamusi massifs in the eastern segment of the Central Asian Orogenic Belt: Geochronological and geochemical evidence from granitoids and rhyolites. Journal of Asian Earth Sciences, 49: 234 – 248
Wang F, Xu WL, Gao FH, Zhang HH, Pei FP, Zhao L and Yang Y.

2014. Precambrian terrane within the Songnen-Zhangguangcai Range Massif, NE China: Evidence from U-Pb ages of detrital zircons from the Dongfengshan and Tadong groups. Gondwana Research, 26(1): 402 – 413

Wang F, Xu WL, Xing KC, Wang YN, Zhang HH, Wu W, Sun CY and Ge WC. 2019. Final closure of the Paleo-Asian Ocean and onset of subduction of Paleo-Pacific Ocean: Constraints from Early Mesozoic magmatism in central southern Jilin Province, NE China. Journal of Geophysical Research: Solid Earth, 124(3): 2601 – 2622

Wang PJ, Liu WZ, Wang SX and Song WH. 2002. $^{40}Ar/^{39}Ar$ and K/Ar dating on the volcanic rocks in the Songliao basin, NE China: Constraints on stratigraphy and basin dynamics. International Journal of Earth Sciences, 91(2): 331 – 340

Wang PJ, Chen FK, Chen SM, Siebel W and Satir M. 2006a. Geochemical and Nd-Sr-Pb isotopic composition of Mesozoic volcanic rocks in the Songliao basin, NE China. Geochemical Journal, 40(2): 149 – 159

Wang PJ, Mattern F, Didenko NA, Zhu DF, Singer B and Sun XM. 2016. Tectonics and cycle system of the Cretaceous Songliao Basin: An inverted active continental margin basin. Earth-Science Reviews, 159: 82 – 102

Wang YL, Zhang CJ and Xiu SZ. 2001. Th/Hf-Ta/Hf identification of tectonic setting of basalts. Acta Petrologica Sinica, 17(3): 413 – 421 (in Chinese with English abstract)

Wang YN, Xu WL, Wang F and Li XB. 2018. New insights on the Early Mesozoic evolution of multiple tectonic regimes in the northeastern North China Craton from the detrital zircon provenance of sedimentary strata. Solid Earth, 9(6): 1375 – 1397

Wilde SA and Zhou JB. 2015. The Late Paleozoic to Mesozoic evolution of the eastern margin of the Central Asian Orogenic Belt in China. Journal of Asian Earth Sciences, 113: 909 – 921

Winchester JA and Floyd PA. 1977. Geochemical discrimination of different magma series and their differentiation products using immobile elements. Chemical Geology, 20: 325 – 343

Wooden JL, Czamanske GK, Fedorenko VA, Arndt NT, Chauvel C, Bouse RM, King BSW, Knight RJ and Siems DF. 1993. Isotopic and trace-element constraints on mantle and crustal contributions to Siberian continental flood basalts, Noril'sk area, Siberia. Geochimica et Cosmochimica Acta, 57(15): 3677 – 3704

Workman RK and Hart SR. 2005. Major and trace element composition of the depleted MORB mantle (DMM). Earth and Planetary Science Letters, 231(1 – 2): 53 – 72

Wu FY, Sun DY, Li HM, Jahn BM and Wilde S. 2002. A-type granites in northeastern China: Age and geochemical constraints on their petrogenesis. Chemical Geology, 187(1 – 2): 143 – 173

Wu FY, Yang JH, Lo CH, Wilde SA, Sun DY and Jahn BM. 2007. The Heilongjiang Group: A Jurassic accretionary complex in the Jiamusi Massif at the western Pacific margin of northeastern China. Island Arc, 16(1): 156 – 172

Wu FY, Sun DY, Ge WC, Zhang YB, Grant ML, Wilde SA and Jahn BM. 2011. Geochronology of the Phanerozoic granitoids in northeastern China. Journal of Asian Earth Sciences, 41(1): 1 – 30

Wu FY, Yang JH, Xu YG, Wilde SA and Walker RJ. 2019. Destruction of the North China Craton in the Mesozoic. Annual Review of Earth and Planetary Sciences, 47(1): 173 – 195

Wu TT, Zhou YH, Chen C, Liu K, Bao QZ, Wu DT and Chai L. 2018. Geochronology and geochemistry of the Early Cretaceous basalt in the Genhe area, northern Great Xing'an Range and geological implications. Geology and Exploration, 54(6): 1270 – 1281 (in Chinese with English abstract)

Xiao WJ, Windley BF, Hao J and Zhai MG. 2003. Accretion leading to collision and the Permian Solonker suture, Inner Mongolia, China: Termination of the central Asian orogenic belt. Tectonics, 22(6): 8

Xiao WJ, Windley BF, Huang BC, Han CM, Yuan C, Chen HL, Sun M, Sun S and Li JL. 2009. End-Permian to mid-Triassic termination of the accretionary processes of the southern Altaids: Implications for the geodynamic evolution, Phanerozoic continental growth, and metallogeny of Central Asia. International Journal of Earth Sciences, 98(6): 1189 – 1217

Xu JF, Wang Q and Yu XY. 2000. Geochemistry of high-Mg andesites and adakitic andesite from the Sanchazi block of the Mian-Lue ophiolitic melange in the Qinling Mountains, central China: Evidence of partial melting of the subducted Paleo-Tethyan crust. Geochemical Journal, 34(5): 359 – 377

Xu JF, Shinjo R, Defant MJ, Wang Q and Rapp RP. 2002. Origin of Mesozoic adakitic intrusive rocks in the Ningzhen area of East China: Partial melting of delaminated lower continental crust? Geology, 30(12): 1111 – 1114

Xu WL, Ji WQ, Pei FP, Meng E, Yu Y, Yang DB and Zhang XZ. 2009. Triassic volcanism in eastern Heilongjiang and Jilin provinces, NE China: Chronology, geochemistry, and tectonic implications. Journal of Asian Earth Sciences, 34(3): 392 – 402

Xu WL, Pei FP, Wang F, Meng E, Ji WQ, Yang DB and Wang W. 2013. Spatial-temporal relationships of Mesozoic volcanic rocks in NE China: Constraints on tectonic overprinting and transformations between multiple tectonic regimes. Journal of Asian Earth Sciences, 74: 167 – 193

Xu WL, Wang F, Pei FP, Meng E, Tang J, Xu MJ and Wang W. 2013. Mesozoic tectonic regimes and regional ore-forming background in NE China: Constraints from spatial and temporal variations of Mesozoic volcanic rock associations. Acta Petrologica Sinica, 29(2): 339 – 353 (in Chinese with English abstract)

Yang WB, Niu HC, Cheng LR, Shan Q and Li NB. 2015a. Geochronology, geochemistry and geodynamic implications of the Late Mesozoic volcanic rocks in the southern Great Xing'an Mountains, NE China. Journal of Asian Earth Sciences, 113: 454 – 470

Yang YT, Guo ZX, Song CC, Li XB and He S. 2015b. A short-lived but significant Mongol-Okhotsk collisional orogeny in latest Jurassic-earliest Cretaceous. Gondwana Research, 28(3): 1096 – 1116

Ying JF, Zhou XH, Zhang LC and Wang F. 2010. Geochronological framework of Mesozoic volcanic rocks in the Great Xing'an Range, NE China, and their geodynamic implications. Journal of Asian Earth Sciences, 39(6): 786 – 793

Yuan W, Xu XH, Lu JL, Yang ZY, Wang BH and Zhu JF. 2014. Zircon SHRIMP dating and Hf isotope compositions of Late Mesozoic volcanic rocks from Changling fault depression, Songliao Basin, and their geological implications. Geological Bulletin of China, 33(10): 1473 – 1481 (in Chinese with English abstract)

Zhang JH, Ge WC, Wu FY, Wilde SA, Yang JH and Liu XM. 2008. Large-scale Early Cretaceous volcanic events in the northern Great Xing'an Range, northeastern China. Lithos, 102(1 – 2): 138 – 157

Zhang XX, Su Z and Gao YF. 2017. Zircon U-Pb geochronology and geochemistry of the Early Cretaceous volcanic rocks from the Manitu Formation in the Hongol Area, northeastern Inner Mongolia. Acta Geologica Sinica, 91(4): 1286 – 1304

Zhou JB, Wang B, Wilde SA, Zhao GC, Cao JL, Zheng CQ and Zeng WS. 2015. Geochemistry and U-Pb zircon dating of the Toudaoqiao blueschists in the Great Xing'an Range, Northeast China, and tectonic implications. Journal of Asian Earth Sciences, 97: 197 – 210

Zhu JX, Wang CM, Chen Q, Shi KX, Duan HY and Li QX. 2022. Geochemical and fluid evidences for fluorine-rich magmatic-hydrothermal origin of the giant Chalukou Mo deposit in the northeast China. Ore Geology Reviews, 141: 104679

附中文参考文献

崔玉斌, 王凯, 何付兵, 尹刚伟, 王召林, 王广磊, 折士焜. 2021. 大兴安岭北段奇力滨地区玛尼吐组火山岩年代学、地球化学特征及其构造意义. 地质学报, 95(11): 3301 – 3316

葛文春, 隋振民, 吴福元, 张吉衡, 徐学纯, 程瑞玉. 2007. 大兴安岭东北部早古生代花岗岩锆石 U-Pb 年龄、Hf 同位素特征及地质意义. 岩石学报, 23(2): 423 – 440

侯贺晟, 王成善, 张交东, 马峰, 符伟, 王璞珺, 黄永建, 邹长春, 高有峰, 高远, 张来明, 杨璠, 国瑞. 2018. 松辽盆地大陆深部科学钻探地球科学研究进展. 中国地质, 45(4): 641 – 657

裴福萍, 许文良, 杨德彬, 纪伟强, 于洋, 张兴洲. 2008. 松辽盆地南部中生代火山岩: 锆石 U-Pb 年代学及其对基底性质的制约. 地球科学, 33(5): 603 – 617

瞿雪姣, 王璞珺, 高有峰, 万晓樵. 2014. 松辽盆地断陷期火石岭组时代归属探讨. 地学前缘, 21(2): 234 – 250

汪云亮, 张成江, 修淑芝. 2001. 玄武岩类形成的大地构造环境的 Th/Hf-Ta/Hf 图解判别. 岩石学报, 17(3): 413 – 421

吴涛涛, 周永恒, 陈聪, 刘凯, 鲍庆中, 吴大天, 柴璐. 2018. 大兴安岭北段根河地区早白垩世玄武岩年代学、地球化学及其地质意义. 地质与勘探, 54(6): 1270 – 1281

许文良, 王枫, 裴福萍, 孟恩, 唐杰, 徐美君, 王伟. 2013. 中国东北中生代构造体制与区域成矿背景: 来自中生代火山岩组合时空变化的制约. 岩石学报, 29(2): 339 – 353

袁伟, 徐旭辉, 陆建林, 杨振宇, 王保华, 朱建锋. 2014. 松辽盆地长岭断陷晚中生代火山岩 SHRIMP 锆石 U-Pb 测年、Hf 同位素组成及其地质意义. 地质通报, 33(10): 1473 – 1481